International Journal of Nanomedicine Dovepress

Open Access Full Text Article ORIGINAL RESEARCH

Hyaluronic Acid-Modified and Doxorubicin-Loaded Au Nanorings for Dual-Responsive and Dual-Imaging Guided Targeted Synergistic Photothermal Chemotherapy Against Pancreatic Carcinoma

Lingyu Hu*, Zhengwei Song*, Bin Wu, Xiaodan Yang, Fei Chen, Xiaoguang Wang

Department of Surgery, The Second Affiliated Hospital of Jiaxing University, Jiaxing, 314000, People's Republic of China

*These authors contributed equally to this work

Correspondence: Fei Chen; Xiaoguang Wang, Department of Surgery, The Second Affiliated Hospital of Jiaxing University, No. 1518, Huancheng North Road, Jiaxing, 314000, People's Republic of China, Tel +86-0573-82080930, Email tangchouer@163.com; wangxiaoguang@zjxu.edu.cn

Introduction: Pancreatic carcinoma (PC) is a highly malignant digestive tumor. Nanotechnology-based minimally invasive techniques have been proposed to provide a new opportunity for PC treatment.

Methods: A minimally invasive nanoplatform (named HA/DOX-AuNRs) is fabricated by HA modifying and DOX loading Au nanorings (AuNR). Because of their complicated geometric structure and tunable localized surface plasmon resonance peak in the second near-infrared laser window (NIR-II window), HA/DOX-AuNRs exhibit fluorescence/photoacoustic and photothermal properties, dual-responsive DOX release, and tumor-targeting ability. HA/DOX-AuNRs are expected to improve the tumor therapeutic efficiency and reduce undesirable side effects through fluorescence/photoacoustic dual-imaging guided targeted synergetic photothermal chemotherapy under NIR-II irradiation.

Results: The morphological and physicochemical properties of HA/DOX-AuNRs are well-examined at first. The cytotoxicity, cellular uptake, and in vitro therapeutic effect of fluorescence/photoacoustic dual-imaging guided targeted synergetic photothermal chemotherapy are evaluated in Panc-1 cells. The in vivo biodistribution, anticancer effects, and systemic toxicity are investigated using PC xenograft models.

Discussion: HA/DOX-AuNRs significantly improve the therapeutic efficacy in a dual-responsive and dual-imaging guided targeted synergy.

Kewords: pancreatic carcinoma, Au nanorings, DOX, NIR-II, photothermal therapy, chemotherapy

Introduction

Pancreatic carcinoma (PC) is a digestive system tumor with a high malignancy and a poor prognosis worldwide.[1,2] Although surgical treatment, chemotherapy, and radiotherapy have made notable progress, the 5-year survival rate of patients with PC has not increased significantly.[3,4] Minimally invasive techniques offer a promising alternative for unresectable PC. However, their clinical applications are limited due to non-specific damage and low efficiency. To overcome these obstacles, researchers improve minimally invasive therapeutic procedures by focusing on targeted killing of tumor cells with minimum dose and side effects.[5] In recent years, research on nanomedicines for cancer treatment has undergone unprecedented developments.[6,7] Nanotechnology-based minimally invasive techniques have been proposed to alter the conventional therapeutic pattern and provide a new opportunity for PC treatment.

Various nanoparticle-mediated minimally invasive techniques enhance the antitumor efficacy using multipronged tumor-specific approaches.[8–10] Recently, the photoacoustic imaging-guided synergistic photothermal chemotherapy triggered by near-infrared (NIR) laser has been proven to be a minimally invasive strategy in preclinical and clinical investigations of malignant tumors.[11,12] Compared with the traditional first NIR window (NIR-I window, 650–950 nm), the second NIR

Received: 5 May 2024
Accepted: 5 December 2024
Published: 14 December 2024

window (NIR-II window, 1000–1350 nm) is much more suitable for minimally invasive techniques (NIR-I window, 650–950 nm), because it provides deeper tissue penetration and higher photoexcitation efficiency.[13–15] Therefore, NIR-II provides photothermal chemotherapy with maximal antitumor efficacy and minimal adverse effects.[16,17] However, nanomaterials for photoacoustic imaging guided synergistic photothermal chemotherapy triggered by an NIR-II laser are rarely reported.[18] To date, the development of a nanoplatform for photoacoustic imaging guided synergistic photothermal chemotherapy using NIR-II lasers remains challenging.

Au nanoparticles (AuNPs) are ideal nanoplatforms for biological applications because of their good biocompatibility and tunable localized surface plasmon resonance (LSPR) properties.[19,20] Nowadays, some special nanostructured AuNPs, such as Au nanobipyramids and Au nanorods, are ideal candidates with photoacoustic and photothermal properties in the NIR-II window, because of their strong local electric-field enhancements and high molar extinction coefficients. Although various types of AuNPs have been reported, only a few exhibit LSPR peaks in the NIR-II window.[21,22] Therefore, the development of novel NIR-II window-responsive AuNPs is highly desirable. Thus, Au nanorings (AuNRs) are an appropriate choice because of their complicated geometric structure and strong LSPR effect.[23] The structurally complicated AuNRs not only obtain the desired LSPR peak, but also provide the site for surface modification and drug loading.[24] Therefore, it is feasible to prepare an AuNR-based nanoplatform for photoacoustic imaging guided synergistic photothermal chemotherapy using NIR-II laser. Hence, the preparation and modification of AuNRs are highly desirable for minimally invasive PC treatment.

Several wet-chemical strategies have been developed to prepare AuNRs.[25] AuNRs are varied by manipulating the deposition rate, and its LSPR peak can be controlled in the range of 780–1350 nm.[26,27] Furthermore, hyaluronic acid (HA) is an ideal candidate to modify AuNRs due to its good biocompatibility, biodegradability, and low toxicity. In recent studies, various HA-modified AuNPs achieved tumor targeting by combining enhanced permeability and retention (EPR)-mediated passive targeting and HA-mediated active targeting.[28,29] Moreover, due to the abundance of hydroxyl and carboxyl groups, HA not only represents multiple sites for loading different drugs (such as doxorubicin, DOX, an antitumor drug), but also exhibits the responsive drug release ability of the tumor acidic microenvironment and high temperature.[30–32] Furthermore, DOX provides the feasibility of fluorescence imaging. Therefore, the combination of AuNRs, HA and DOX is highly potential and desirable for the development of a tumor-targeted and dual-responsive "all-in-one" nanoplatform for fluorescence/photoacoustic dual-imaging guided targeted synergistic photothermal chemotherapy in the NIR-II window against PC.

In this study, complicated geometric structure AuNRs are prepared using nanorod-templated method with a complicated geometric structure and a tunable LSPR peak in the NIR-II window, which are then used to fabricate a minimally invasive nanoplatform (HA/DOX-AuNRs) by HA modification and DOX loading. HA/DOX-AuNRs are expected to improve tumor therapeutic efficiency and reduce the undesirable side effects of fluorescence/photoacoustic dual-imaging guided targeted synergistic photothermal chemotherapy using NIR-II irradiation (Scheme 1). The physicochemical properties of HA/DOX-AuNRs are well-examined at first. The cytotoxicity, cellular uptake, and in vitro therapeutic effect of targeted synergistic photothermal chemotherapy are evaluated in Panc-1 cells. In vivo biodistribution, anticancer effects, and systemic toxicity are investigated in tumor-bearing mice. The results of both in vitro/vivo studies support that HA/DOX-AuNRs significantly improve the therapeutic efficacy in a dual-responsive and dual-imaging guided targeted synergy.

Experimental Sections

Preparation and Characterization of HA/DOX-AuNRs

The fabrication of HA/DOX-AuNRs was divided into AuNR and HA/DOX-AuNR preparation according to the report method with some modifications.[33,34] In AuNR preparation, Te nanorods were synthesized by co-educing Te and Se precursors, and then were used as template to prepare AuNRs via galvanic replacement reaction and nanoscale Kirkendall effect. The LSPR peaks of AuNRs was adjusted by adding $HAuCl_4$, and they were monitored by UV-vis spectroscopy (Varian Cary, CA). Subsequently, HA-modified AuNRs were prepared by a nanoprecipitation method. Briefly, HA (100 kDa), AuNRs, EDC·HCl and ADH were dissolved in water and followed by 30 min reaction, and 50 mL of acetone was added and allowed to react overnight. After the organic layer was evaporated, the HA-modified AuNRs were obtained by ultrafiltration and dialysis against deionized water. Finally, HA/DOX-AuNRs were fabricated after DOX incubated with HA-modified AuNRs (The molar ratio DOX: HA was 50:1).

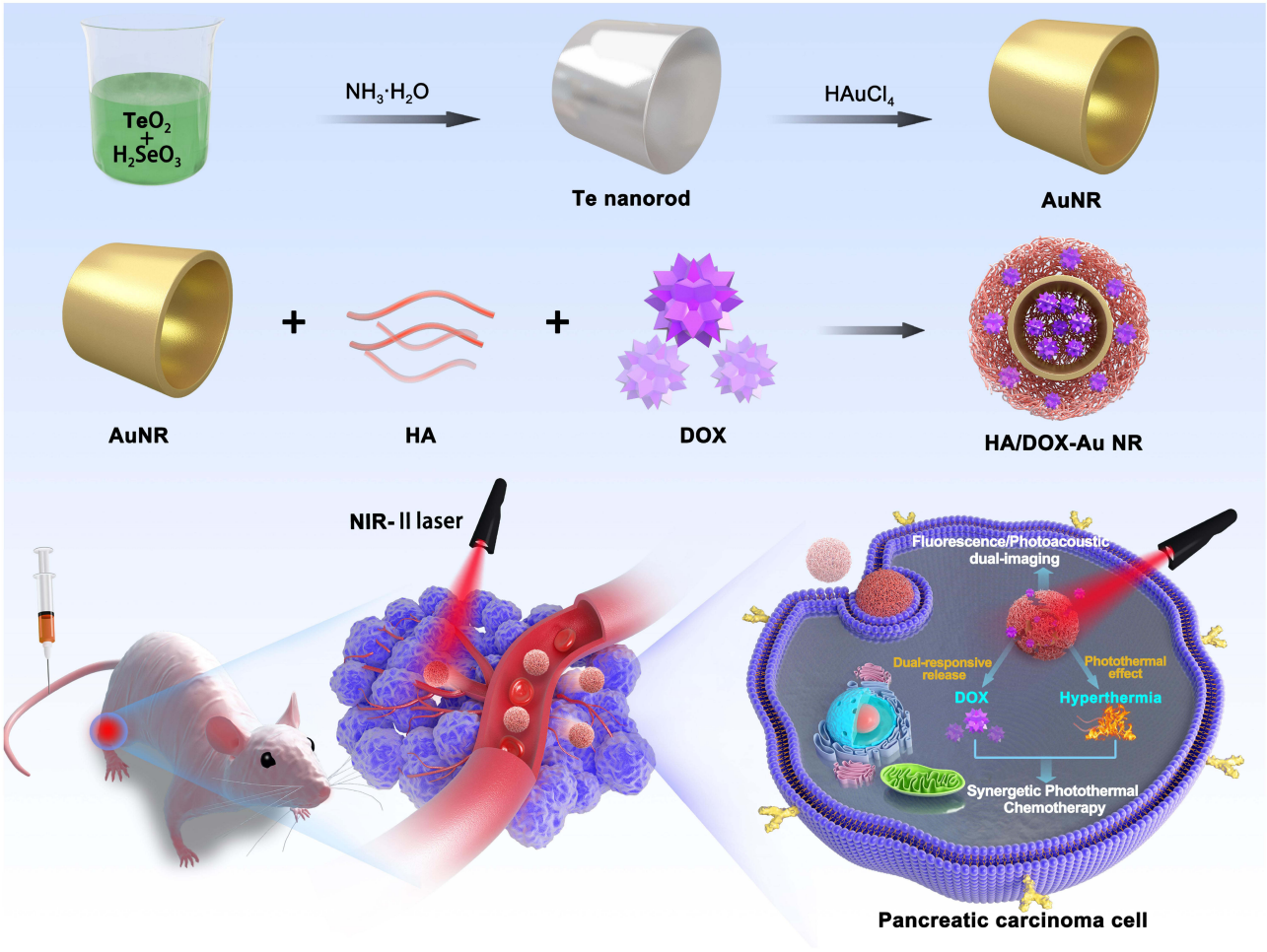

Scheme 1 Schematic representation of HA/DOX-AuNRs for dual-responsive and dual imaging guided targeted synergetic photothermal chemotherapy against pancreatic carcinoma.

Characterization of HA/DOX-AuNRs

For evaluation of morphology, and energy dispersive X-ray (EDX) elemental mapping, HA/DOX-AuNRs were characterized by transmission electron microscope (TEM, JEM-2100F, JEOL, Japan) and scanning electron microscopy (SEM, JSM-6360LA, Japan). The average size and zeta potential were measured by dynamic light scattering (DLS) using a particle sizer (NICOMP 380 ZLS, FL, USA).

To measure the photothermal effect, HA/DOX-AuNRs, AuNRs and DOX were placed in quartz cuvettes and irradiated with NIR-II irradiation (1064 nm, 2.0 W/cm^2) for 5 min. During the irradiation, temperature was monitored with infrared thermal camera every 0.5 min. To clarify the influence of Au concentration on the photothermal heating effect, HA/DOX-AuNRs with different concentrations (1, 20, and 20 μg/mL of Au) were conducted with different NIR-II irradiation time (0, 2, 4, and 6 min). The pH-dependent release of DOX was evaluated in aqueous solutions at different pH values (5.0 and 7.4). The temperature-dependent DOX release was evaluated by exposing the sample to NIR-II (1064 nm, 2.0 W/cm2) for 5 min before each time point. A dialysis method (MWCO 3500–5000) was used to investigate the release behavior of DOX from HA/DOX-AuNRs, and the DOX concentration was measured by high-pressure liquid chromatography. The loading efficiency was calculated according to the equation: loading efficiency (%) = (weight of detected DOX /weight of added DOX) × 100%.

To explore the photothermal conversion efficiency (η) of HA/DOX-AuNRs according to Korgel's method, another cycle of laser irradiation was performed on HA/DOX-AuNRs under the same conditions. Detailed calculation was given as following:

$$\eta = \frac{hA\left(\Delta T_{max} - \Delta T_{max,PBS}\right)}{I\left(1 - 10^{-A_\lambda}\right)}$$

where h was the heat transfer coefficient of the system, A was the surface area of samples, ΔT_{max} was the maximum temperature of the hydrogel rising under irradiation, $\Delta T_{max,\mathrm{PBS}}$ was the ambient temperature during the photothermal experiment, I is the power of the 808 nm laser used, A_λ was the absorbance value of the sample at 808 nm.

Cell Culture and Establishment of PC Xenograft Models

The pancreatic cancer cells, Panc-1, were purchased from Chinese Academy of Sciences and selected for the in vitro cell experiments. Panc-1 cells were cultured in DMEM supplemented with 10% fetal bovine serum, 100 units of potassium penicillin and 100 μg of streptomycin sulfate per 1 mL of culture media at 37°C in 5% CO_2.

Male BALB/c nude mice (6–8 weeks old and 18–22 g weight, purchased from Shanghai LAC Laboratory Animal Co. Ltd) were housed in a SPF grade animal center. To obtain PC xenograft models, Panc-1 cells (5×10^6) were injected subcutaneously into the right rear-flank area of the mice. Further, the tumor growth was evaluated using a caliper, and tumor volumes were measured by formula: $V = (L \times W^2)/2$ (L: length of the tumor; W: width of the tumor). When the tumors approached a volume larger than 80 mm^3, PC xenograft models were successfully fabricated for in vivo studies. All animal experiments were conducted in compliance with the relevant laws and institutional guidelines and approved by the ethics committee of Jiaxing University Medical College (JUMC2022-167).

Cell Viability

The biocompatibility of HA/DOX-AuNRs was assessed using Panc-1. Briefly, cells were seeded in 96-well plates and treated with HA/DOX-AuNRs for 24 h. Then, viability was measured using a Cell Counting Kit-8 (CCK-8), and expressed as a percentage normalized to the value of Control.

Cellular Uptake

Panc-1 cells were seeded onto 28-mm glass cover slips for 24 h. The cells were incubated with HA/DOX-AuNRs for 6 h, washed twice with PBS, and fixed with a 4% paraformaldehyde solution. DAPI was used to stain nuclei, and slides were rinsed thrice with PBS. Confocal laser scanning microscopy (CLSM; Leica TCS SP8, Germany) was used to detect cellular uptake and distribution of HA/DOX-AuNRs. Furthermore, 3D multicellular tumor spheroids (3D MCTS) with Panc-1 cells were used to assess the delivery and penetration efficacy of HA/DOX-AuNRs to mimic the tumor microenvironment. Panc-1 cells were seeded in a special 96-well plate for 48 h. DOX and HA/DOX-AuNRs were added to the medium for 12 h in the dark, and the fluorescence of cellular DOX in 3D MCTS was obtained using CLSM.

In vitro Study on Photothermal Chemotherapy

To evaluate synergistic chemo-phototherapy, Panc-1 cells were cultured with HA/DOX-AuNRs, AuNRs, and DOX for 24 h, followed by irradiation with NIR-II (1064 nm, 8 min, 2.0 W/cm^2). To verify the therapeutic effects, calcein-acetoxymethyl ester (calcein AM) and propidium iodide (PI) were used to recognize surviving and apoptotic cells, respectively. One fraction of the cells was identified by CLSM, and the others were harvested for analysis following apoptosis by flow cytometry. Furthermore, Panc-1 cells were cultured in glass-bottomed cell culture dishes for 24 h. After different treatments, cells were labeled with immunofluorescence of γH2AX. Nuclei were stained with DAPI and imaged using CLSM. The Panc-1 cells in 96 plates were then incubated with HA/DOX-AuNRs, AuNRs, and DOX at different concentration for 24 h, and then the medium was replaced with 200 μL of fresh medium. After NIR-II irradiation (1064 nm, 8 min, 2.0 W/cm^2), cells in each group were further incubated for 24 h. Cell viability was evaluated using the Cell Counting Kit-8 (CCK-8).

In vivo Fluorescence/Photoacoustic Dual-Imaging

PC xenograft models in each group were injected with 1 mL HA/DOX-AuNRs, AuNRs, or DOX through the tail vein. The fluorescence imaging was monitored at 0, 12, 24, and 36 h using a small animal in vivo imaging system at the

appropriate wavelengths. Mice were sacrificed after 24 h and tumor tissues were collected. The amount of gold in the tumors was quantified using inductively coupled plasma mass spectrometry (ICP-MS). The photoacoustic imaging of tumor region was determined using a multimode small animal photoacoustic/ultrasonic imaging system under 945 nm laser at a given time points (0, 12, 24 and 36 h).

In vivo Antitumor Study

The PC xenograft models were divided into four groups (n = 6 per group). The mice were injected with HA/DOX-AuNRs, AuNRs, DOX, or saline via the tail vein six times every three days. The day following injection, the tumors were irradiated with a NIR-II laser (1064 nm, 2.0 W/cm^2, 8 min). The in vivo photothermal effects were evaluated using a thermal camera. Briefly, after intravenous injections at different times, the tumor region was exposed to an NIR-II laser (1064 nm, 2.0 W/cm^2) for 5 min of irradiation with a 1-min rest interval. Temperature variations in the tumors were dynamically monitored using an infrared thermal imaging camera. Following irradiation, tumor size and body weight were recorded. The mice were sacrificed after 21 days of treatment, and the primary tumors along with the organs (heart, liver, lungs, kidneys, and spleen) were surgically excised and stained with hematoxylin and eosin (HE) for optical microscopy. TUNEL and Ki-67 expression was evaluated by immunofluorescence using purified primary and biotinylated secondary antibodies.

Statistical Analysis

Data are presented as mean ± SD unless otherwise indicated. Differences between groups were examined using the Student's *t*-test. Statistical significance was established at $p < 0.05$.

Results and Discussions

Preparation and Characterization

AuNRs were prepared through a Te nanorod-template method. The Te nanorod were solid structure as shown in TEM image (Figure 1A). After Au deposition, AuNRs had good dispersibility and morphological uniformity as expected (Figure 1B). In HA/DOX-AuNRs, the complicated geometric structure was not affected by the modification of HA and loading of DOX, and EDS mapping also indicate the Te has been removed (Figure 1C and D). The SEM image of HA/DOX-AuNRs strongly supports the theory that HA was successfully coated in AuNRs (Figure 1E). DLS measurements indicated that the HA/DOX-AuNRs had a lager particle size distribution than AuNRs (167 ± 31.5 nm vs 131 ± 17.6 nm), further suggesting HA was successfully coated in AuNRs (Figure 1F). In the zeta potential analysis, HA/DOX-AuNRs were more negative than AuNRs (−19.5 ± 3.3 mv vs −10 ± 2.3 mv), because of HA modification. Furthermore, the modification of HA endows HA/DOX-AuNRs with enhanced stability in both PBS and serum after 7 days (data not shown). The DOX loading and LSPR effects were further assessed using UV-vis absorption spectroscopy, which demonstrated a similar plasmon resonance peak at approximately 1195 nm (Figure 1G). After modification, the HA/DOX-AuNRs presented a peak corresponding to DOX and a slight redshift of the LSPR peak at 1160 nm (~65 nm). Furthermore, the DOX peak indicated that DOX was successfully loaded into HA/DOX-AuNRs through the interaction of HA and the complicated geometric structure of the AuNRs.

The photothermal effect and dual-responsive DOX release were further studied by dynamically detecting the variations in temperature and DOX concentration. The temperature of HA/DOX-AuNRs, AuNRs and DOX suspensions reached 52.4, 52.1 and 35.7 °C after 5 min of NIR-II irradiation, respectively. (Figure 2A). In addition, infrared images provided evidence that HA/DOX-AuNRs had concentration- and irradiation time-dependent photothermal characteristics (Figure 2B). The photostability of HA/DOX-AuNRs was further investigated under NIR-II irradiation and cooling cycles. Notably, after four cycles, there was no observable attenuation in the photothermal property of HA/DOX-AuNRs (Figure 2C). The dual-responsive release of DOX was studied under different pH values and NIR irradiation conditions (Figure 2D). Almost 50% of the encapsulated DOX was released at pH 5.0 within 8 h, whereas only ~20% was released at pH 7.4. Furthermore, NIR irradiation induced heating could accelerate the release of DOX from HA/DOX-AuNRs. These results were attributed to the acidic microenvironment and heating loosened the HA structure, exposing more DOX

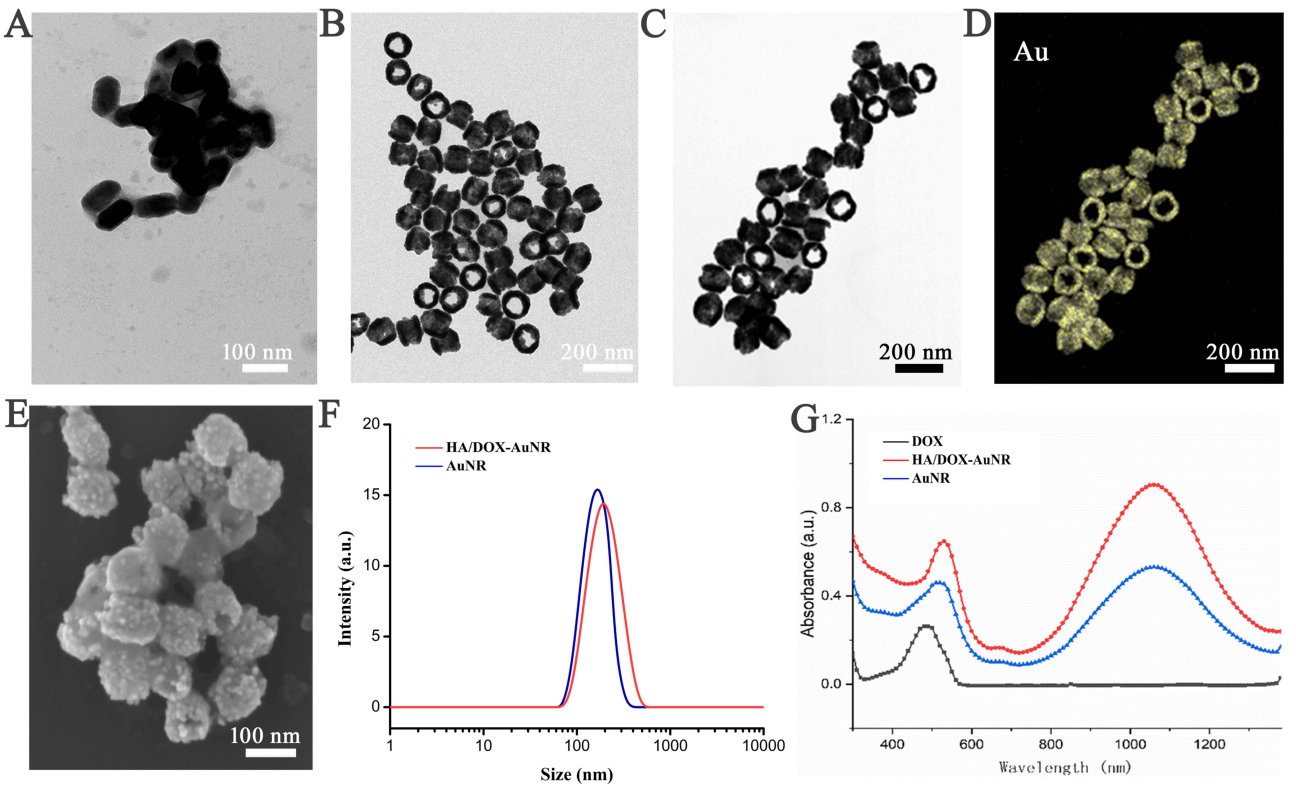

Figure 1 (**A**–**C**) TEM images of TeSe nanorods, AuNRs and HA/DOX-AuNR; (**D**) EDS mapping of HA/DOX-AuNR; (**E**) SEM images of HA/DOX-AuNR; (**F** and **G**) Particle size distributions and UV-Vis absorption spectra.

molecules to the external environment.[35] To investigate their photothermal activities, photothermal conversion experiments were conducted. Upon photoirradiation using under NIR-II irradiation for 300 s, the photothermal conversion performance of HA/DOX-AuNRs grew as time increasing (Figure 2E). Based on the result, photothermal conversion efficiency of HA/DOX-AuNRs was calculated as 45.8% (Figure 2F). Therefore, the dual-responsive DOX release property was of great significance in cancer therapy, which reduced undesired drug release during transportation in the blood circulation. Meanwhile, the excellent photothermal conversion performance making HA/DOX-AuNRs the most suitable candidate for the following PTT study.

Cellular Uptake

Before assessing the combined therapeutic potential of HA/DOX-AuNRs, the viability of Panc-1 cells treated with HA/DOX-AuNRs, AuNRs and DOX was determined using CCK-8 assays. Without NIR irradiation, HA/DOX-AuNRs showed negligible toxicity toward Panc-1 cells throughout the concentration range studied, as DOX was gradually released from HA/DOX-AuNRs inside cells (Figure 3A). The cellular uptake was assessed using CLSM and 3D MCTS. The CLSM images revealed that the fluorescence intensity of cancer cells treated with HA/DOX-AuNRs was stronger than cells treated with DOX, demonstrating that HA/DOX-AuNRs could effectively deliver DOX into cancer cells (Figure 3B and C). 3D MCTS generated from Panc-1 cells was used to investigate the efficacy of HA/DOX-AuNRs delivery, because it could mimic the microenvironment of solid tumors in vitro.[36] As shown in the horizontal sectional fluorescence images of MCTS, the penetration depth of DOX was significantly increased using HA/DOX-AuNRs compared to free DOX, indicating the enhanced delivery and penetrating capacity of HA/DOX-AuNRs (Figure 3D). This improved drug delivery, attributed to the interaction between HA in HA/DOX-AuNRs and CD44 on the cell surface. These results suggested that HA/DOX-AuNRs were effectively taken up by PC cells to provide targeted photothermal chemotherapy.

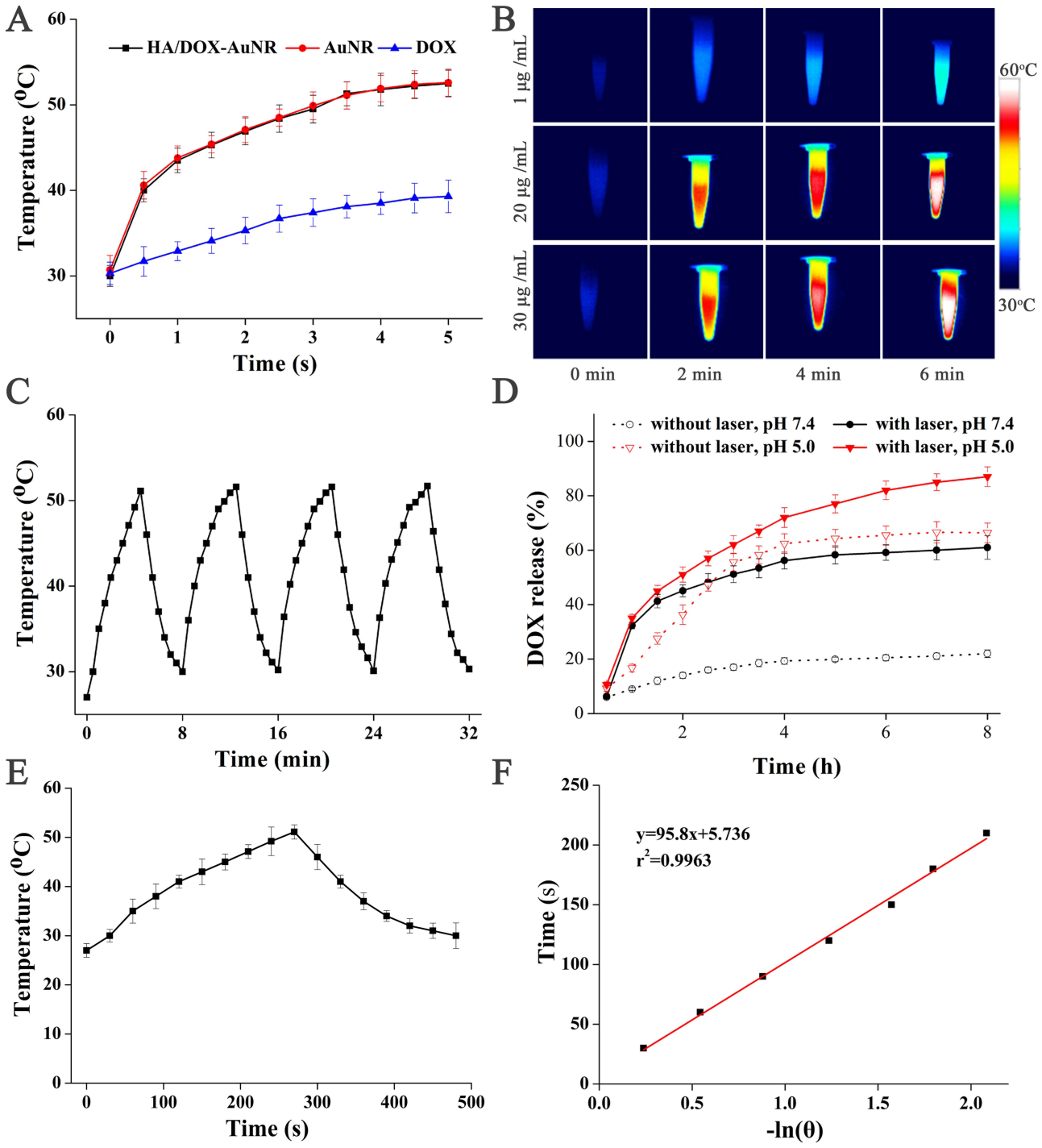

Figure 2 (**A**) Photothermal curves of HA/DOX-AuNRs, AuNRs and DOX irradiated by NIR-II for different time (The equivalent Au concentration was 20 μg/mL); (**B**) Corresponding infrared thermal images of HA/DOX-AuNRs with different concentration and irradiation time; (**C**) Photothermic stability for 4 heating and cooling cycles; (**D**) Release behaviors of DOX from HA/DOX-AuNRs at pH 5.0 and 7.4 with/without NIR-II irradiation; (**E** and **F**) heating and cooling curve and linear time data vs −lnθ of HA/DOX-AuNRs with NIR-II irradiation.

In vitro Photothermal Chemotherapy Studies

To explore the targeted synergetic photothermal chemotherapy effect, the viability of Panc-1 cells treated with HA/DOX-AuNRs, AuNRs and DOX was determined using CCK-8 at first. In the case of NIR irradiation, cell viability remarkably decreased when Au concentration more than 20 μg/mL, demonstrating the high photothermal efficacy of

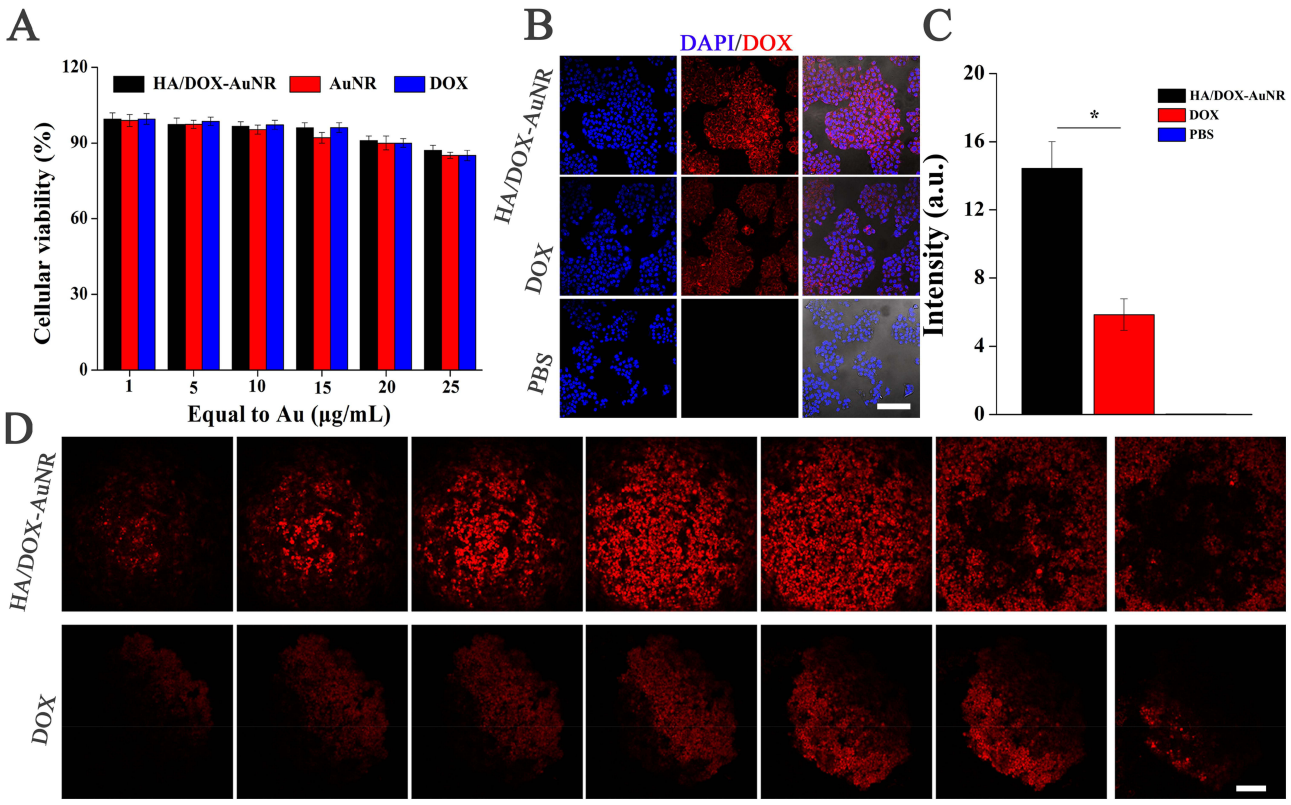

Figure 3 (**A**) Viability of Panc-1 cells incubated with different concentrations of HA/DOX-AuNRs, AuNRs and DOX in the absence of NIR-II irradiation; (**B** and **C**) CLSM images and quantitative analysis of cellular uptake (Scale bar = 500 μm, *: p<0.05); (**D**) CLSM images of 3D MCTS after treated 12 h (Scale bar = 500 μm).

HA/DOX-AuNRs (Figure 4A). HA/DOX-AuNRs always exhibited greater toxicity than AuNRs and DOX, resulting from targeted cellular internalization and dual-responsive DOX release. Furthermore, the therapeutic efficacy of photothermal chemotherapy was studied using calcein AM, and the changing trend of the fluorescence pattern was like that of the CCK-8 results (Figure 4B). As expected, NIR irradiation caused the obvious death of cells treated with HA/DOX-AuNRs, and a clear demarcation line was observed between the dead and live cell (green) regions. Apoptotic effects were also investigated by flow cytometry analysis of Annexin V-FITC/PI double-stained cells (Figure 4C). HA/DOX-AuNRs irradiation group showed a higher percentage of total apoptotic cells than other groups, further confirming the synergetic targeting effect of photothermal chemotherapy. T The mechanism of Panc-1 cell death was studied by inhibiting DNA repair pathways. γH2AX, a key protein in DNA repair, was used to assess DNA damage in cells after various treatments (Figure 4D). Immunofluorescence of γH2AX foci indicated that treatment with AuNRs or DOX alone did not inhibit single DNA repair pathway.[37] In contrast, HA/DOX-AuNRs were more effective in inhibiting a single DNA repair pathway, which is consistent with the experimental cytotoxicity results. Therefore, these results supported that HA/DOX-AuNRs could effectively inhibit Panc-1 cell growth by inhibiting DNA repair pathway through dual-responsive DOX release and targeted synergetic photothermal chemotherapy.

In vivo Fluorescence/Photoacoustic Dual-Imaging

Nanoparticle-based targeted drug delivery is a key precondition for successful nanoparticle-based targeted drug delivery and anticancer treatment and promises sustained accumulation of HA/DOX-AuNRs in tumors. Therefore, the in vivo tumor fluorescence imaging of HA/DOX-AuNRs in PC xenograft models was studied after intravenous injection at first (Figure 5A). Weak fluorescence was observed in the tumor region 12 h after intravenous injection in all groups.

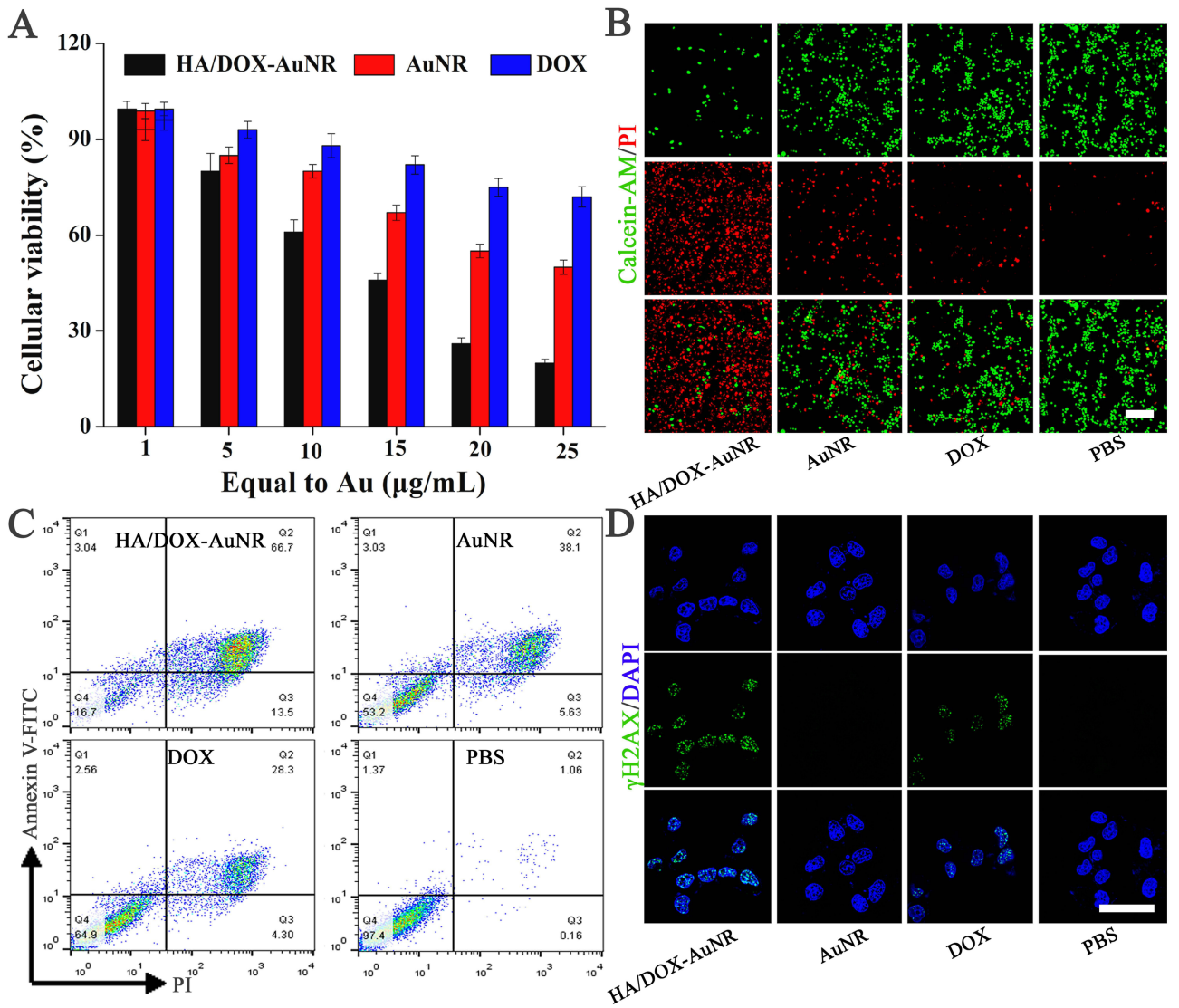

Figure 4 (**A**) Viability of Panc-1 cells incubated with different concentrations of HA/DOX-AuNRs, AuNRs and DOX in presence of NIR-II irradiation; (**B**) Confocal fluorescence images of Calcein AM/PI-stained and Panc-1 cells treated with HA/DOX-AuNRs, AuNRs and DOX with NIR-II laser irradiation (Au concentration was 20 μg/mL, (Scale bar = 200 μm)); (**C**) Apoptotic effects of different treatments; (**D**) CLSM images of γH2AX foci (green) in cell nuclei (blue) in treated Panc-1 cells with NIR-II laser irradiation (Scale bar = 50 μm).

Moreover, there was gradual enhancement in the fluorescence signal within the tumor over time, reaching a peak approximately 24 h post-injection. HA/DOX-AuNRs showed fluorescence much stronger at the tumor site at the same time than other groups, indicating that HA/DOX-AuNRs presented tumor-targeting capacity that benefited from HA. ICP-MS analysis indicated that accumulation efficacy of HA/DOX-AuNRs in tumor was 11.3%, approximately 3-fold higher than AuNRs, further confirming the tumor-targeting delivery ability of HA/DOX-AuNRs (Figure 5B). The in vivo tumor photoacoustic imaging was also studied. Similar as fluorescence results, photoacoustic signal of tumor region gradually increased with over time and a strong signal was seen even at 24 h after intravenous injection (Figure 5C and D). There were strong photoacoustic signals even after 36 h, demonstrating the long intratumoral retention time of HA/DOX-AuNRs. Therefore, the results indicated that HA/DOX-AuNRs could accumulate in the tumor tissue and realize fluorescence/photoacoustic dual-imaging guided targeted photothermal chemotherapy.

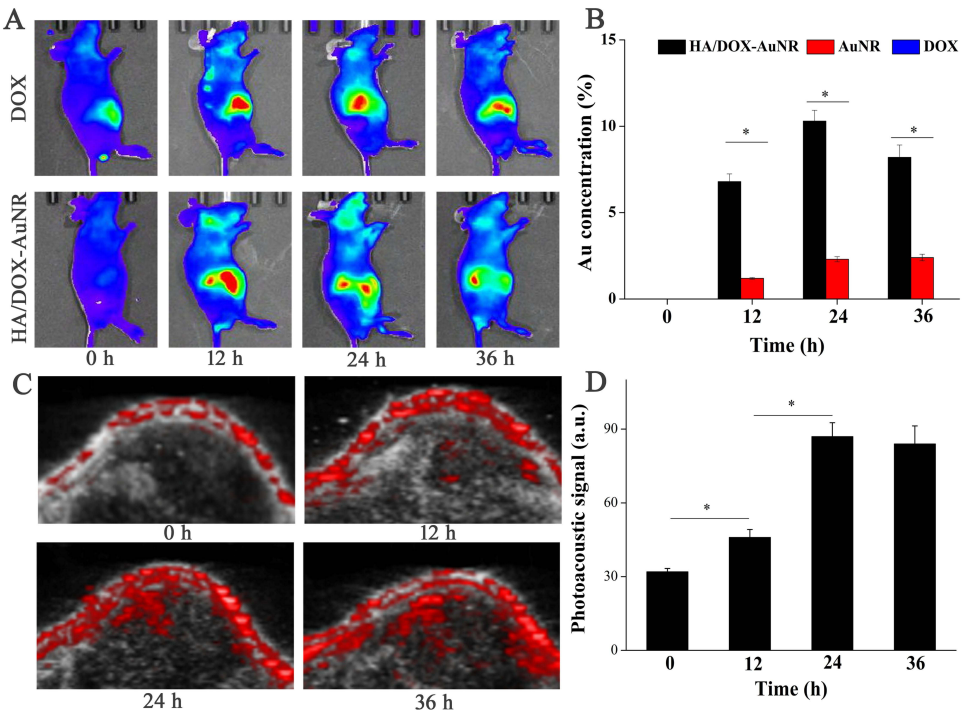

Figure 5 (**A**) Fluorescence images of PC xenograft models before and after intravenous injections of HA/DOX-AuNRs and DOX; (**B**) ICP-MS results of Au concentration in tumor tissues before and after intravenous injections of HA/DOX-AuNRs (*: p<0.05); (**C** and **D**) Photoacoustic imaging and signal intensity of tumor tissue before and after intravenous injection of HA/DOX-AuNRs (*: p<0.05).

In vivo Photothermal Chemotherapy

The minimum threshold temperature for photothermal therapy of tumors is usually regarded as 45 °C, so the effects of in vivo photothermal effect of HA/DOX-AuNRs were investigated at first.[38] After 24 h of intravenous injection, temperature variations in the tumors were recorded by infrared thermal imaging camera (Figure 6A). In HA/DOX-AuNR group, the temperature quickly reached 44.8 °C, causing irreversible damage to tumors. In contrast to the AuNR and DOX groups, the temperature increased to 42.1 °C and 36.5 °C, respectively. The antitumor efficacy was assessed by monitoring survival status, body weight and tumor volume during the therapeutic period. As expected, mice treated with HA/DOX-AuNRs exhibited the best survival rate among all groups (Figure 6B). There was no significant body weight difference in all groups, supporting the negligible systemic toxicity of HA/DOX-AuNRs (Figure 6C). However, tumor volume displayed different outcomes. DOX and AuNRs had an inhibitory effect on the tumors by decreasing the tumor volume in the first 3 days, but no obvious therapeutic effect was observed because the tumor volume increased. In contrast, the tumor in HA/DOX-AuNR group was much smaller (Figure 6D). After 21 days of treatment, the excised major organs and tumors were processed for histological analysis (Figure 6E). TUNEL immunofluorescence staining showed more dead cancer cells (green) in the HA/DOX-AuNR group than in the other groups. According to HE staining, there was a mass of necrotic tumor tissue in the cancerous region from HA/DOX-AuNR group, and the tumor cells retained their normal morphology and structure in other groups. Furthermore, immunohistochemical staining for Ki-67 protein revealed that the number of proliferating cancer cells in HA/DOX-AuNR group was significantly lower than in the other groups, which was consistent with the antitumor results. Therefore, HA/DOX-AuNRs significantly improved antitumor efficacy, most likely due to their enhanced tumor-targeting ability, dual-responsive release, and fluorescence/photoacoustic dual-imaging guided synergetic photothermal chemotherapy.

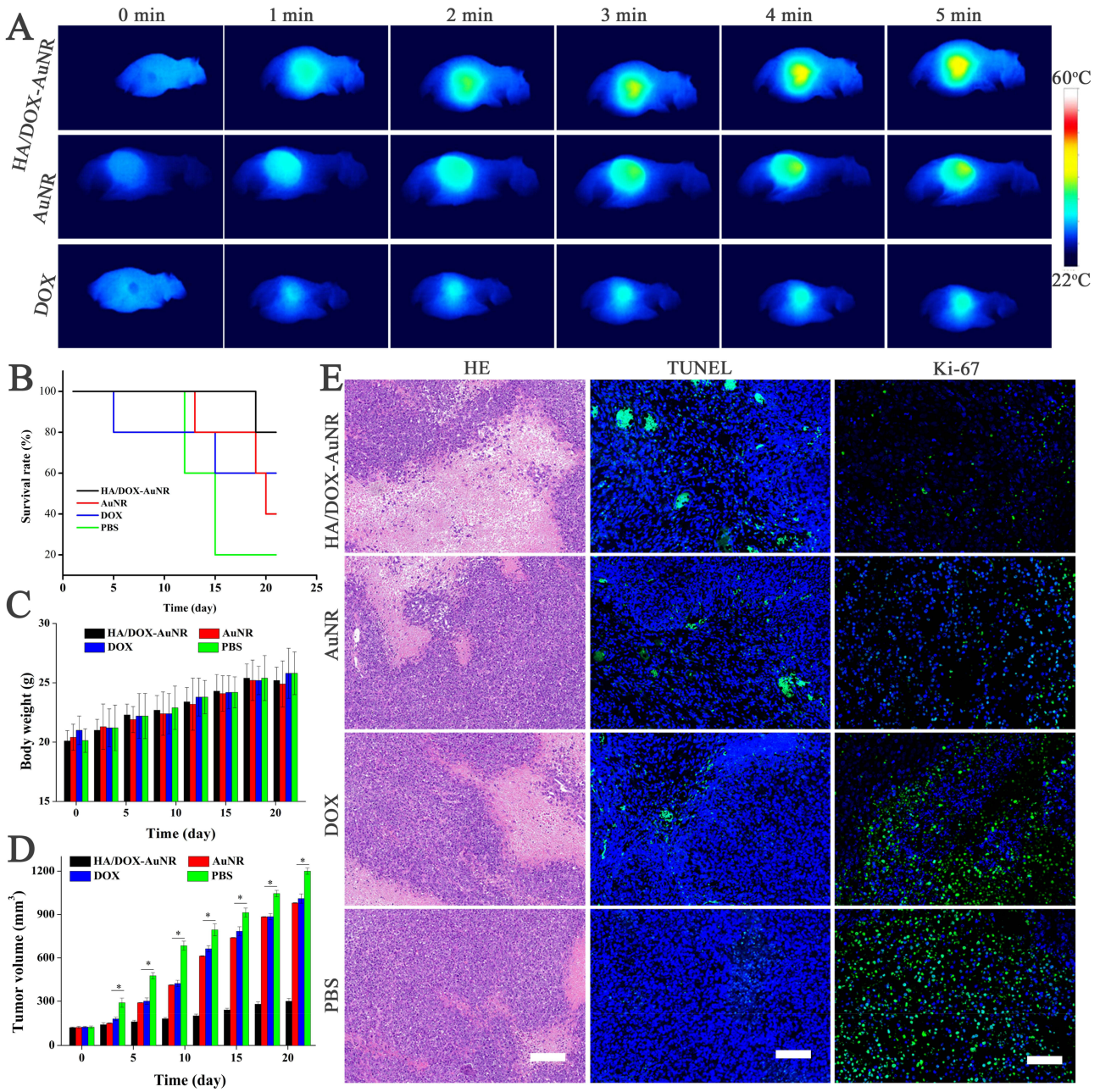

Figure 6 (**A**) Infrared photothermal images of PC xenograft models injected with different agents after exposure to NIR-II irradiation. (**B**–**D**) Survival curves, body weight curves and Tumor volume curves in PC xenograft models after different treatments (*: $p<0.05$); (**E**) Pathological analysis of tumor tissues (Scale bar = 200 μm).

To examine the potential toxic effects of different formulations on the major organs (heart, liver, spleen, lung and kidney), organ samples were histologically analyzed using HE staining (Figure 7). There was significant swelling, vacuolated cells, and rupture of myocardial fibers in the heart tissue of the DOX group, which was attributed to the cardiac toxicity of DOX. No adverse side effects were observed in the AuNR and HA/DOX-AuNR groups. Therefore, these results demonstrated that HA/DOX-AuNRs exhibited powerful fluorescence/photoacoustic dual-imaging guided targeted synergetic therapeutic efficacy against PC without serious side effects.

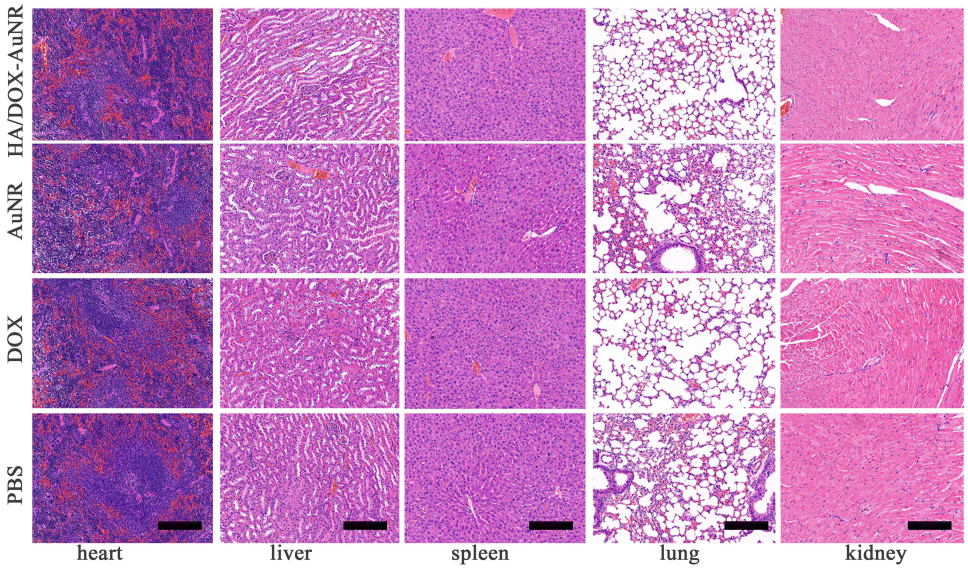

Figure 7 Images of HE stained tissue sections of heart, liver, spleen, lung, and kidney of models after different treatments (Scale bar = 200 μm).

Conclusions

A novel minimally invasive nanoplatform, HA/DOX-AuNRs, was successfully developed for dual-responsive and dual-imaging guided targeted synergetic photothermal chemotherapy against PC. Thanks to the anisotropic morphology of AuNRs and modification of HA, HA/DOX-AuNRs exhibited the ability of dual-responsive release and targeted photothermal chemotherapy in NIR-II window. According to the results of in vitro/vivo studies, HA/DOX-AuNRs could accumulate in tumors through EPR effects and HA-assisted tumor targeting, showing pH and temperature dual-responsive DOX release. Furthermore, photothermal chemotherapy exhibited the synergistic therapeutic efficacy without severe side effects to normal tissues. This study demonstrates the immense potential of HA/DOX-AuNRs in PC therapy and provides insights into the design of multifunctional minimally invasive nanoplatforms to maximize therapeutic efficacy and minimize side effects.

Data Sharing Statement

The datasets generated during the current study are available from the corresponding author.

Ethics Approval and Consent to Participate

The animal experiment of this study was approved by the Experimental Animal Ethics Committee of Jiaxing University Medical College (JUMC2022-167), and carried out in the animal room of Jiaxing University.

Author Contributions

All authors made a significant contribution to the work reported, whether that is in the conception, study design, execution, acquisition of data, analysis and interpretation, or in all these areas; took part in drafting, revising or critically reviewing the article; gave final approval of the version to be published; have agreed on the journal to which the article has been submitted; and agree to be accountable for all aspects of the work.

Funding

This research was supported by Zhejiang Provincial Natural Science Foundation of China (Grant No. LY21H160046) and funding from Traditional Chinese Medicine Science and Technology Planning Project of Zhejiang Province (Grant NO. 2022ZQ073) and the science and technology planning project of Jiaxing City (No. 2022AZ10009, 2024AZ30002).

Disclosure

The authors declare no conflict of interest.

References

1. Pandya G, Kirtonia A, Singh A, et al. A comprehensive review of the multifaceted role of the microbiota in human pancreatic carcinoma. *Semin Cancer Biol*. 2022;86(Pt 3):682–692. doi:10.1016/j.semcancer.2021.05.027
2. Cao X, Hu Y, Luo S, et al. Neutrophil-mimicking therapeutic nanoparticles for targeted chemotherapy of pancreatic carcinoma. *Acta Pharm Sin B*. 2019;9(3):575–589. doi:10.1016/j.apsb.2018.12.009
3. Cheng MY, Zeng Y, Sun Y, et al. Preliminary analysis of the expression of ZBTB1 in human pancreatic carcinoma. *J Cell Mol Med*. 2021;25 (17):8573–8576. doi:10.1111/jcmm.16804
4. Yamashita Y, Kitano M, Ashida R. Value of endoscopy for early diagnosis of pancreatic carcinoma. *Dig Endosc*. 2020;32(1):27–36. doi:10.1111/den.13467
5. Nie C, Zhang Y, Zhou G, et al. Analysis of the efficacy of transcatheter arterial infusion chemotherapy in the treatment of pancreatic carcinoma. *J Interv Med*. 2021;4(1):21–26. doi:10.1016/j.jimed.2020.10.005
6. Yang P, Zhi X, Xu Y, Qian L, Dai Z. Nanomedicines enhance minimally invasive therapy of pancreatic cancer. *Nano Today*. 2023;51:101891. doi:10.1016/j.nantod.2023.101891
7. Shang T, Yu X, Han S, Yang B. Nanomedicine-based tumor photothermal therapy synergized immunotherapy. *Biomater Sci*. 2020;8 (19):5241–5259. doi:10.1039/D0BM01158D
8. Yu Y, Fan P, Li J, Wang S. Preparation of biocompatible manganese selenium-based nanoparticles with antioxidant and catalytic functions. *Molecules*. 2023;28(11):4498.
9. Cai H, Wang R, Guo X, et al. Combining gemcitabine-loaded macrophage-like nanoparticles and erlotinib for pancreatic cancer therapy. *Mol Pharm*. 2021;18(7):2495–2506. doi:10.1021/acs.molpharmaceut.0c01225
10. Cai H, Dai X, Guo X, et al. Ataxia telangiectasia mutated inhibitor-loaded copper sulfide nanoparticles for low-temperature photothermal therapy of hepatocellular carcinoma. *Acta Biomater*. 2021;127:276–286. doi:10.1016/j.actbio.2021.03.051
11. Hou G, Qian J, Xu W, et al. Multifunctional PEG-b-polypeptide-decorated gold nanorod for targeted combined chemo-photothermal therapy of breast cancer. *Colloids Surf B*. 2019;181:602–611. doi:10.1016/j.colsurfb.2019.05.025
12. Wang M, Zhang M, Hu X, et al. Lipid-functionalized gold nanorods with plug-to-direct mitochondria targeting ligand for synergetic photothermal-chemotherapy of tumor therapy. *Eur J Pharm Biopharm*. 2023;185:71–81. doi:10.1016/j.ejpb.2023.02.010
13. Pan H, Li S, Kan JL, et al. A cruciform phthalocyanine pentad-based NIR-II photothermal agent for highly efficient tumor ablation. *Chem Sci*. 2019;10(35):8246–8252. doi:10.1039/C9SC02674F
14. Chen K, Fang W, Zhang Q, et al. Tunable NIR absorption property of a dithiolene nickel complex: a promising NIR-II absorption material for photothermal therapy. *ACS Appl Bio Mater*. 2021;4(5):4406–4412. doi:10.1021/acsabm.1c00168
15. Zhang L, Forgham H, Huang X, et al. All-in-one inorganic nanoagents for near-infrared-II photothermal-based cancer theranostics. *Mater Today Adv*. 2022;14:100226. doi:10.1016/j.mtadv.2022.100226
16. Roy S, Bag N, Bardhan S, Hasan I, Guo B. Recent progress in NIR-II fluorescence imaging-guided drug delivery for cancer theranostics. *Adv Drug Deliv Rev*. 2023;197:114821. doi:10.1016/j.addr.2023.114821
17. Wei J, Liu Y, Yu J, et al. Conjugated polymers: optical toolbox for bioimaging and cancer therapy. *Small*. 2021;17(43):e2103127. doi:10.1002/smll.202103127
18. Xie Q, Liu J, Chen B, et al. NIR-II fluorescent activatable drug delivery nanoplatform for cancer-targeted combined photodynamic and chemotherapy. *ACS Appl Bio Mater*. 2022;5(2):711–722. doi:10.1021/acsabm.1c01139
19. Wang Y, Meng HM, Li Z. Near-infrared inorganic nanomaterial-based nanosystems for photothermal therapy. *Nanoscale*. 2021;13(19):8751–8772. doi:10.1039/D1NR00323B
20. Wang J, Wu X, Shen P, et al. Applications of inorganic nanomaterials in photothermal therapy based on combinational cancer treatment. *Int J Nanomed*. 2020;15:1903–1914. doi:10.2147/IJN.S239751
21. Si P, Razmi N, Nur O, et al. Gold nanomaterials for optical biosensing and bioimaging. *Nanoscale Adv*. 2021;3(10):2679–2698. doi:10.1039/D0NA00961J
22. Yang Y, Wang H. The golden age: shining the light on theragnostics. *Adv Nanobiomed Res*. 2021;1(8):2000103. doi:10.1002/anbr.202000103
23. Yoo S, Go S, Son J, et al. Au nanorings with intertwined triple rings. *J Am Chem Soc*. 2021;143(37):15113–15119. doi:10.1021/jacs.1c05189
24. Chu CK, Tu YC, Hsiao JH, et al. Combination of photothermal and photodynamic inactivation of cancer cells through surface plasmon resonance of a gold nanoring. *Nanotechnology*. 2016;27(11):115102. doi:10.1088/0957-4484/27/11/115102
25. Lin X, Liu Y, Lin M, Zhang Q, Nie Z. Synthesis of circular and triangular gold nanorings with tunable optical properties. *Chem Commun*. 2017;53 (78):10765–10767. doi:10.1039/C7CC06024F
26. Hu Y, Yang Y, Wang H, Du H. Synergistic integration of layer-by-layer assembly of photosensitizer and gold nanorings for enhanced photodynamic therapy in the near infrared. *ACS nano*. 2015;9(9):8744–8754. doi:10.1021/acsnano.5b03063
27. Mu S, Chen H, Shi C, Zhang J, Yang B. Au nanoring arrays with tunable morphological features and plasmonic resonances. *Nano Res*. 2021:1–6.
28. Hejazi M, Arshadi S, Amini M, et al. Hyaluronic acid-functionalized gold nanoparticles as a cancer diagnostic probe for targeted bioimaging applications. *Microchem J*. 2023;193:108953. doi:10.1016/j.microc.2023.108953
29. Sakurai Y, Harashima H. Hyaluronan-modified nanoparticles for tumor-targeting. *Expert Opin Drug Deliv*. 2019;16(9):915–936. doi:10.1080/17425247.2019.1645115
30. Lee C-S, Kim T, Kang Y, et al. Targeted drug delivery nanocarriers based on hyaluronic acid-decorated dendrimer encapsulating gold nanoparticles for ovarian cancer therapy. *Mater Today Chem*. 2022;26:101083. doi:10.1016/j.mtchem.2022.101083
31. Yim MS, Hwang YS, Bang JK, et al. Morphologically homogeneous, pH-responsive gold nanoparticles for non-invasive imaging of HeLa cancer. *Nanomedicine*. 2021;34:102394. doi:10.1016/j.nano.2021.102394

32. Xu W, Qian J, Hou G, et al. Hyaluronic acid-functionalized gold nanorods with pH/NIR dual-responsive drug release for synergetic targeted photothermal chemotherapy of breast cancer. *ACS Appl Mater Interfaces*. 2017;9(42):36533–36547. doi:10.1021/acsami.7b08700
33. Cai K, Zhang W, Foda MF, et al. Miniature hollow gold nanorods with enhanced effect for in vivo photoacoustic imaging in the NIR-II window. *Small*. 2020;16(37):e2002748. doi:10.1002/smll.202002748
34. Cai K, Zhang W, Zhang J, Li H, Han H, Zhai T. Design of gold hollow nanorods with controllable aspect ratio for multimodal imaging and combined chemo-photothermal therapy in the second near-infrared window. *ACS Appl Mater Interfaces*. 2018;10(43):36703–36710. doi:10.1021/acsami.8b12758
35. You J, Zhang G, Li C. Exceptionally high payload of doxorubicin in hollow gold nanospheres for near-infrared light-triggered drug release. *ACS nano*. 2010;4(2):1033–1041. doi:10.1021/nn901181c
36. Tan H, Liu Y, Hou N, et al. Tumor microenvironment pH-responsive pentagonal gold prism-based nanoplatform for multimodal imaging and combined therapy of castration-resistant prostate cancer. *Acta Biomater*. 2022;141:408–417. doi:10.1016/j.actbio.2022.01.012
37. Xiong Y, Wang W, Deng Q, et al. Mild photothermal therapy boosts nanomedicine antitumor efficacy by disrupting DNA damage repair pathways and modulating tumor mechanics. *Nano Today*. 2023;49:101767. doi:10.1016/j.nantod.2023.101767
38. Li Z, Yin S, Cheng L, Yang K, Li Y, Liu Z. Magnetic targeting enhanced theranostic strategy based on multimodal imaging for selective ablation of cancer. *Adv Funct Mater*. 2014;24(16):2312–2321. doi:10.1002/adfm.201303345